FLight Biofabrication Supports Maturation of Articular Cartilage with Anisotropic Properties

Puiggalí-Jou, Anna ; Rizzo, Riccardo ; Bonato, Angela ; Fisch, Philipp ; Ponta, Simone ; Weber, Daniel M ; Zenobi-Wong, Marcy

DOI: https://doi.org/10.1002/adhm.202302179

ADVANCED HEALTHCARE MATERIALS
www.advhealthmat.de

FLight Biofabrication Supports Maturation of Articular Cartilage with Anisotropic Properties

*Anna Puiggalí-Jou, Riccardo Rizzo, Angela Bonato, Philipp Fisch, Simone Ponta, Daniel M. Weber, and Marcy Zenobi-Wong**

Tissue engineering approaches that recapitulate cartilage biomechanical properties are emerging as promising methods to restore the function of injured or degenerated tissue. However, despite significant progress in this research area, the generation of engineered cartilage constructs akin to native counterparts still represents an unmet challenge. In particular, the inability to accurately reproduce cartilage zonal architecture with different collagen fibril orientations is a significant limitation. The arrangement of the extracellular matrix (ECM) plays a fundamental role in determining the mechanical and biological functions of the tissue. In this study, it is shown that a novel light-based approach, Filamented Light (FLight) biofabrication, can be used to generate highly porous, 3D cell-instructive anisotropic constructs that lead to directional collagen deposition. Using a photoclick-based photoresin optimized for cartilage tissue engineering, a significantly improved maturation of the cartilaginous tissues with zonal architecture and remarkable native-like mechanical properties is demonstrated.

1. Introduction

Traumatic injuries, joint diseases, aging, and obesity are some of the conditions which are increasing the need for cartilage repair solutions. Since cartilage lacks self-repair capabilities, tissue engineering technologies present a great opportunity to fulfil this need.[1–5] Cartilage is an avascular, aneural, and alymphatic tissue composed of chondrocytes embedded in a dense extracellular matrix (ECM) that mainly consists of collagen type II and proteoglycans.[6] Although it seems to be a simple tissue, faithfully resembling articular cartilage with tissue engineering strategies remains an unmet challenge. Despite major advances in cell sourcing, culture conditions, and supporting biomaterials, a native-like 3D cartilaginous tissue with anisotropic architecture has yet to be obtained.[2,3,6]

Articular cartilage has a distinctive zonal organization, with superficial, middle, and deep zones varying in structure and function (**Figure 1**A).[7–9] The superficial zone of the joint consists of flat chondrocytes embedded in a thin layer of ECM, mainly composed of collagen fibrils running parallel to the articular surface, thus conferring protection to deeper layers from shear-stress. The middle zone comprises sparsely distributed rounded chondrocytes in a proteoglycan-rich ECM and random collagen fibril distribution. The deep zone is characterized by a columnar arrangement of chondrocytes and thick collagen fibrils running perpendicular to the articular surface. Due to its composition and structural organization, the deep zone is crucial in providing the distinctive high compressive resistance of the tissue.[10] The middle zone does not possess this distinctive fibril orientation and can be more easily obtained with homogeneous hydrogels and current tissue engineering methods, including bulk hydrogels,[11,12] granular hydrogels,[13,14] fiber mats,[15–18] and foams,[15,19–22] but superficial and deep zones require technologies that can direct aligned ECM deposition on a cellular scale.

The generation of anisotropic, physical guiding constructs has been demonstrated with 3D printed scaffolds,[23,24] electrospinning,[15] or with the use of directionally frozen scaffolds.[19,20,25] However, these approaches are limited to cell seeding after printing. Cell-laden biofabrication methods, such as extrusion printing in the presence of shear-aligning fibers,[26,27] sizing,[28] or ultrasound-assisted cell patterning[29] have recently emerged, to replace the more limited approaches.

A. Puiggalí-Jou, R. Rizzo, A. Bonato, P. Fisch, S. Ponta, M. Zenobi-Wong
Tissue Engineering + Biofabrication Laboratory
Department of Health Sciences & Technology
ETH Zürich
Otto-Stern-Weg 7, Zürich 8093, Switzerland
E-mail: marcy.zenobi@hest.ethz.ch

R. Rizzo
John A. Paulson School of Engineering and Applied Sciences
Harvard University
52 Oxford Street, Cambridge, MA 02138, USA

R. Rizzo
Wyss Institute for Biologically Inspired Engineering
Harvard University
Boston, MA 02115, USA

D. M. Weber
Division of Hand Surgery
University Children's Hospital Zürich
University of Zürich
Zürich 8032, Switzerland

The ORCID identification number(s) for the author(s) of this article can be found under https://doi.org/10.1002/adhm.202302179

DOI: 10.1002/adhm.202302179

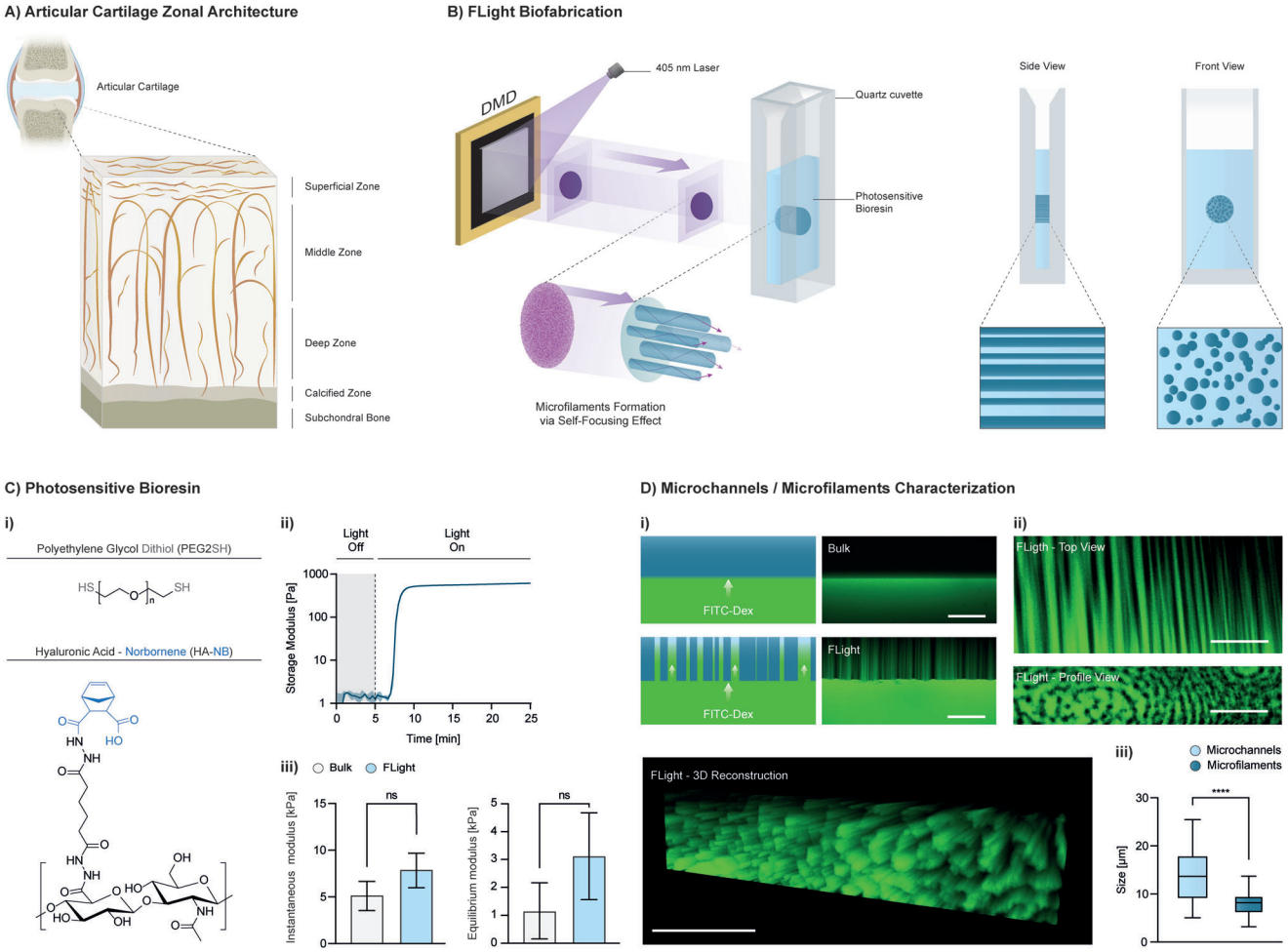

Figure 1. FLight biofabrication of anistropic hydrogels. A) Illustration of the zonal architecture of articular cartilage showing diverse collagen fibril orientation (orange). B) Illustration of FLight working principle. Light projections generated via a digital micromirror device (DMD) are directed toward a quartz cuvette containing the photosensitive bioresin. Due to a phenomenon known as optical modulation instability (OMI), projected laser light has an intrinsic intensity noise speckle pattern that, together with the optical non-linearity of the photoresin, induces a self-focusing effect. This effect eventually results in the formation of microfilaments (blue) and microchannels (light blue, uncrosslinked regions). C-i) Chemical structure of photoresin components highlighting (gray and blue) the reactive groups of the thiol-norbornene step-growth chemistry. ii) Photorheology measurement of optimal photoresin 0.75% HA-NB/0.84% PEG2SH/0.05% LAP. Light exposure (405 nm) was turned on after 5 min triggering the photoclick crosslinking. iii) Comparison of compressive instantaneous and equilibrium moduli of bulk and FLight hydrogels obtained with the same light dose (≈208 mJ cm^{-2}) showing no significant difference. D) Microarchitecture characterization of Flight-generated hydrogel. i) Fluorescently labelled dextran (FITC-Dex, 0.5 MDa) readily (15 min) infiltrated the pores (microchannels) between the microfilaments generated with FLight process. On the other hand, the bulk gels crosslinked with flood LED illumination appeared homogeneous, thus not permitting rapid infiltration of the FITC-Dex solution. Scale bars: 100 µm. ii) Top, profile view and 3D reconstruction of microchannels infiltrated with FITC-Dex (green) and microfilaments (black) for FLight hydrogels (Scale bars: 100 µm). iii) Analysis of microchannels (≈14 ± 5 µm) and microfilaments (≈8 ± 2 µm) size.

Notably, most of the current bioprinting methods rely on bulk hydrogels that consist of a dense polymeric network featuring nanoporous mesh size, thus physically constraining the encapsulated cells and limiting matrix deposition. In the context of cartilage engineering, this often leads to relatively low compressive moduli (a few hundred kPa) compared to native tissue.[27] In contrast to homogeneous hydrogels, the presence of a macroporous network, in addition to improving nutrient diffusion and cell migration potential, can facilitate the deposition of cartilaginous ECM, thus leading to better mechanical properties of the maturing engineered tissue.[30] Importantly, as highlighted by Arora et al., a key role is played by pore shape and distribution, with vertically aligned pores giving higher resistance to compression.[31]

Liu et al. recently introduced a method called Filamented Light (FLight) biofabrication, which can rapidly (in seconds) produce macroporous anisotropic tissues (Figure 1B).[32] Due to a phenomenon known as optical modulation instability (OMI) and the non-linear nature of photosensitive bioresins, FLight generates hydrogels composed of aligned microfilaments and microchannels with diameters ranging from 2 to 30 µm.[32] Such microarchitecture showed excellent cell instructive capabilities in controlling cell and ECM alignment with various cell types. In this work, we leverage FLight's unique potential for generating

anisotropic cartilage constructs that resemble native deep zone ECM composition and architecture and cartilage-like mechanical properties. Additional advances coming from the use of FLight in cartilage engineering include: I) excellent tissue maturation using a relatively low, and more physiological cell concentration compared to current standards (5 vs 20–30 million cells mL^{-1}); II) high-throughput capabilities of the projection-based method (multiple samples in 3.3 s) while guaranteeing excellent cell viability; III) possibility to exploit the flexibility of light projections to form multilayer constructs with distinct architectures; and IV) potential use for clinical setting via in situ procedures.

2. Results and Discussion

2.1. Design and Characterization of Optimized FLight Photoresin for Cartilage Regeneration

FLight biofabrication is a light-based technique and therefore requires the use of photoactivated materials. In recent years, step-growth photocrosslinking mechanisms (i.e., thiol-ene) have become the gold standard, replacing chain-growth mechanisms (i.e., methacryloyl or acrylate-based) for biofabrication methods.[33] Among the various advantages, step-growth reactions are faster, thus requiring less light exposure and lower generation of harmful radicals. They result in more homogeneous networks, are not sensitive to oxygen, and do not form non-biodegradable, hydrophobic kinetic chains. In this work, we chose to use the highly efficient thiol-norbornene photoclick step-growth reaction to crosslink biomaterials optimized for cartilage applications. In the past decades, several synthetic and naturally derived polymers have been studied for their ability to generate hydrogels for cartilage tissue engineering. Among these, HA has arguably shown the most promising results.[11,12,34–38] HA is a native polysaccharide present in human articular cartilage that offers chondrocyte binding sites (via CD44 adhesion receptor) and biodegradability/matrix remodeling potential (via hyaluronidase).[39]

As shown in a previous work,[11] a hydrogel's initial stiffness plays a major role in determining proper tissue maturation. In particular, an initial storage modulus of <1 kPa was found to be optimal for cartilage maturation, resulting in a significant increase in stiffness over the culture period and eventually reaching the range of native cartilage (reported to span from 0.1 to 6.2 MPa).[40–43] In the previous study by Broguiere et al.,[11] enzymatic transglutaminase-crosslinkable high molecular weight HA (HA-TG) was used. In this work we tried to build on the promising results obtained with HA-TG hydrogels by synthesizing an analogous photosensitive suitable for FLight biofabrication and by matching initial mechanical properties. High molecular weight HA (1.5 MDa) was modified with norbornene groups[44] to obtain hyaluronic acid-norbornene (HA-NB) with a similar degree of substitution to HA-TG (HA-NB DS:18% vs HA-TG DS: 13%). As a counterpart for the bifunctional TG peptides, bioinert bifunctional thiolated PEG (PEG2SH) was used (Figure 1C). Various formulations consisting of a 1:1 NB to SH molar ratio and different polymer concentrations were tested by photorheology (data not shown) to fall in the desired range of stiffness (storage modulus <1 kPa). An optimal photoresin was found at 0.75% HANB/ 0.84% PEG2SH, with a plateau storage modulus of 612 ± 11 Pa (Figure 1C-ii). For all the experiments reported in this study, a final concentration of 0.05% of lithium phenyl-2,4,6-trimethylbenzoylphosphinate (LAP) as photoinitiator (PI) was added to the photoresin. LAP was chosen as it is the current standard PI for light-mediated bioprinting, due to its superior water solubility, biocompatibility and absorption in the 360–405 nm range when compared to other PIs such as Irgacure 2959.[33] Dose tests were first performed as previously described to identify the critical gelation threshold (minimum light dose to crosslink the photoresin),[45,46] and thus the optimal printing time which was found to be only 3.3 s. Ellman's test (see Experimental Section) was used to infer the crosslinking efficiency under the optimal light dose (≈208 mJ cm^{-2}) based on residual free thiols in the crosslinked hydrogels, and found to be ≈96%. Highly efficiently crosslinked hydrogels, both for bulk and FLight conditions, showed a comparable ≈250% swelling after equilibrating in PBS for 24 h (Figure S1, Supporting Information).

The mechanical properties of cylindrical samples (2 mm height, 4 mm diameter) obtained with FLight and as bulk with LED flood illumination (using the same light dose) were compared by means of an unconfined compression test showing no significant differences in instantaneous or equilibrium modulus (Figure 1C-iii).

To investigate the microarchitecture of the samples, they were submerged for 15 min in a solution of fluorescently labelled dextran (FITC-Dex, 0.5 MDa), and the presence of microchannels was analyzed by confocal imaging (Figure 1D). As expected, infiltration of FITC-Dex was detected for FLight constructs only, thus revealing the presence of microchannels (≈14 ± 5 μm) that have the potential to enhance nutrient diffusion and guide the deposition of cell-secreted ECM. For the bulk samples, as LEDs are non-coherent light sources that do not show an optical modulation instability (OMI) effect, no microfeatures via self-focusing phenomena could be detected. Only scarce and homogeneous FITC-Dex infiltration was observed, indicating that its penetration was limited to common diffusion processes through the nanoporous polymeric network.

2.2. Cartilage Tissue Maturation

To study the potential of FLight microarchitected constructs in supporting the development of aligned, matured articular cartilage, we embedded human infant polydactyly chondrocytes in the optimized HA-NB/PEG2SH photoresin. Polydactyly chondrocytes have shown proliferation at a steady rate; they produce a cartilage-like matrix and have been extensively investigated as a non-immunogenic, off-the-shelf cell source for potential clinical applications.[47–51] Due to cell-induced light scattering, FLight was found to be limited in maximum cellular concentration. Above a certain threshold, found to be 5 million cells mL^{-1} for the photoresin used in this work, light scattering hinders the formation of microfilaments and microchannels. As shown later, the FLight constructs eventually outperformed most of the current alternatives, despite our having used a low but physiological cell concentration compared to other cartilage biofabrication techniques (hyperphysiologic densities commonly in the range of ≈20–50 million cells mL^{-1}).[26,29] In addition, given the exceptionally high printing speed and the flexibility

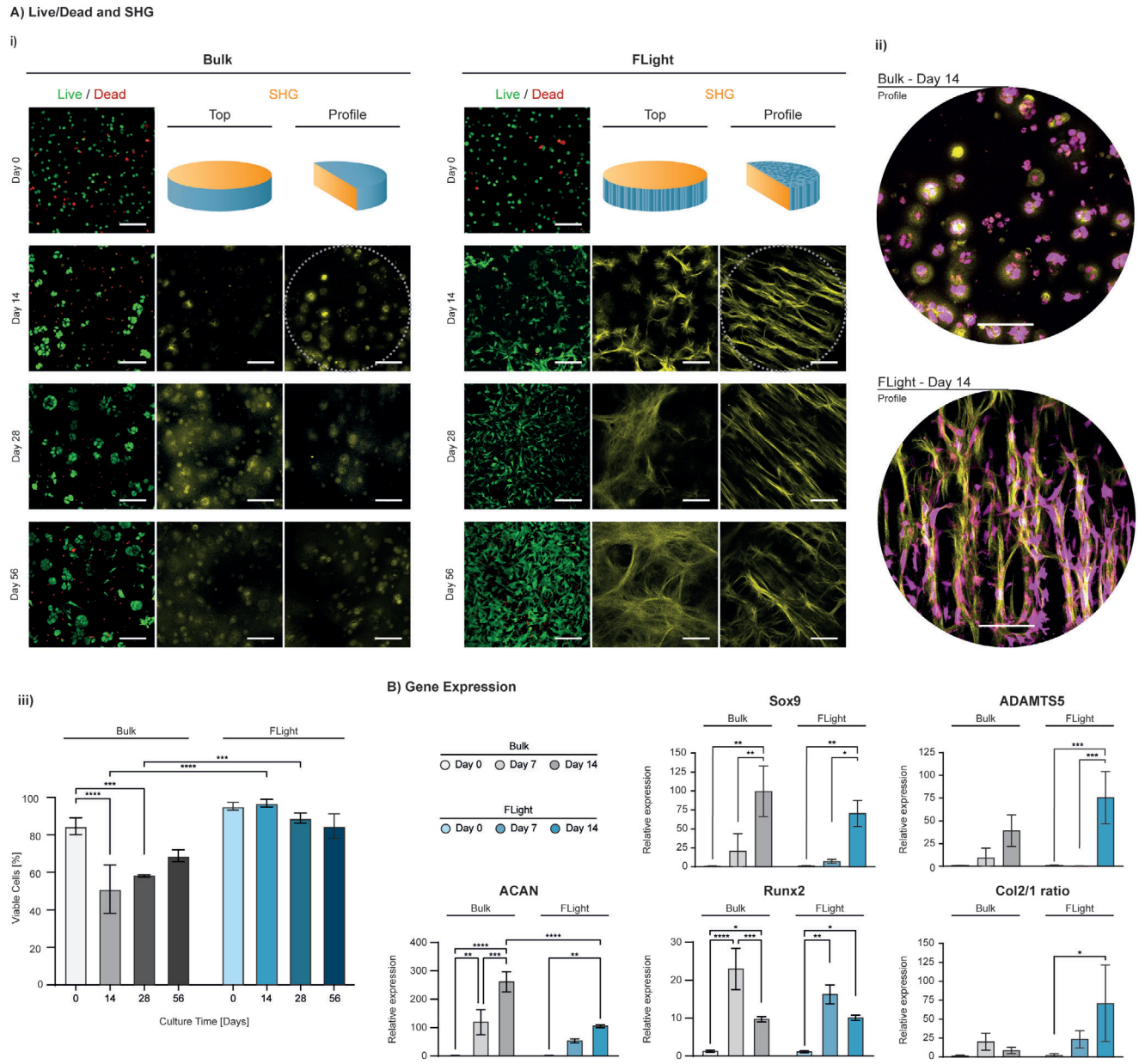

Figure 2. A-i) Panel of live/dead (top view) and second harmonic generation (SHG) imaging for bulk and FLight samples over the course of 2 months of culture. Scale bars: 100 µm. ii) Close-ups of profile view after two weeks of culture (dashed gray circles), highlighting the significant difference in cell (magenta) morphology, distribution, and collagen deposition between the two samples (pericellular for bulk, aligned in the anisotropic FLight construct). Scale bars: 100 µm. iii) Quantification of viable cells over the culturing period. B) Gene expression analysis for chondrogenesis-related genes: Sox9, metalloproteases (ADAMTS5), aggrecan (ACAN), runt-related transcription factor II (Runx2), and ratio of collagen type II versus collagen type I (Col2/1).

imparted by the light-projection design, it was possible to print 10 hydrogels (2 mm height, 4 mm diameter, within the human articular cartilage thickness range) at once (3.3 s total). Modifying the projection lens setup and using a photoresin container with a larger area would permit further improvement of the throughput of this method. Therefore, leveraging the high performance of thiol-norbornene chemistry, FLight represents, to our knowledge, the fastest bioprinting method to generate anisotropic constructs with excellent cell viability (as later shown). Upon printing, the uncrosslinked photoresin was first removed with buffer washing, and bioprinted samples were then placed into chondrogenic media. As controls, the HA-NB/PEG2SH bioresin was cast into cylindrical gels of the same dimensions and crosslinked via LED flood illumination to obtain homogeneous bulk gels.

Live/dead assay was performed directly post-printing (day 0) and after 2, 4, and 8 weeks of culture (**Figure 2**A). FLight resulted in excellent cell viability post-printing (≈95%) and during the culture period (≥85% over 2 months). Viability was found to be generally lower for bulk gels upon crosslinking (≈85%) and

notably reduced after two weeks of culture (≈51%). Although during the 2 months' culture the viability in bulk gels steadily recovered to ≈70%, the significant difference compared to the FLight samples can be attributed to the macroporous architecture of the bulk gels, known to be beneficial for nutrient and oxygen exchange as well as cell spreading and migration. Calcein staining in fact showed that in the microarchitected FLight gels, cells appeared to be more spread and elongated (see also F-actin staining, Figure S2, Supporting Information), while more round and aggregated in the homogeneous bulk gels (Figure 2A-i,ii). Cell proliferation was studied with ki-67 staining (Figure S2, Supporting Information) and showed an increase for both conditions over the course of the first two weeks of culture. Chondrocytes showed a significantly higher proliferation in FLight samples after 14 days compared to the bulk hydrogels, attributable to better cells conditions (higher viability, porosity for nutrient, and oxygen exchange). Importantly, as viability was shown to recover in bulk gels to values comparable to FLight gels, also the cell proliferation seemed to follow a similar trend as later shown by the close total DNA content at the final time point for the two conditions (**Figure 3**B).

The differences in cell behavior and hydrogel, microarchitecture resulted in a significant difference in de novo ECM (neocartilage) deposition. Second harmonic generation (SHG) imaging was performed to monitor the deposition of collagen (Figure 2A-i). As expected, after two weeks of culture, the homogeneous bulk gels did not show aligned collagen deposition, but a rather limited pericellular deposition. In contrast, FLight samples revealed a remarkable anisotropic collagen deposition, with microfilaments acting as physical cell guidance cues and microchannels offering a preferential space for matrix deposition (Figure 2A-ii).

We further investigated the impact of hydrogel architecture (FLight vs bulk) on chondrogenesis by looking at the gene expression level with qPCR over the course of the first two weeks of culture (Figure 2B). The analysis showed for both samples a general increase over time of Sox9, a key chondrogenesis transcription factor which induces the expression of cartilage-related genes such as collagen II. The metallopeptidase ADAMTS5, which can serve as an indicator of ongoing matrix remodeling, was found to be significantly upregulated in FLight samples after two weeks of culture suggesting that the macroporous, aligned microarchitecture of these construct induces a higher matrix remodeling. Aggrecan was also found to follow an upregulation trend over the analyzed culturing period, with a significantly higher expression in the bulk gels after 14 days. However, as later shown in Figure 3, the deposition of aggrecan after two months of culture was found to be significantly higher for FLight samples. Runx2, transcription factor associated with chondrocyte hypertrophy and osteoblast differentiation, was shown to be transiently upregulated after one week and found to decrease after two weeks. This trend has been previously observed with hydrogel embedded chondrocytes and associated with the normal process of chondrocytes maturation. The later decrease in Runx2 expression suggests a maintenance of a stable cartilage phenotype as also inferable based on absence of hypertrophic chondrocytes, and excellent articular cartilage-like maturation (especially in FLight samples) as later shown in Figure 3. Finally, the ratio of collagen type II, main structural component of articular cartilage, and collagen type I, mostly found in fibrocartilage, was found to significantly increase over time for FLight samples indicating good chondrogenic induction. Overall, qPCR suggested that the infant chondrocytes embedded in the optimized photoclick photoresin proposed in this work undergo chondrogenesis induction in the first two weeks of culture.

To evaluate how this induction then translated into neocartilage deposition, and to further investigate the effect of bulk and FLight microarchitecture histological and immunohistological staining were performed after one and two months of culture (Figure 3A). In line with qPCR findings, collagen I content was found to be significantly less pronounced (as desired) in FLight samples compared to bulk. On the other hand, after two months of culture, collagen II and glycosaminoglycans (GAGs) staining were found to be significantly more intense in FLight gels, closely resembling human articular cartilage control. As first observed with SHG (Figure 2A), collagen deposition was confirmed to be hindered by the homogeneous polymeric network and thus mostly deposited pericellularly in the bulk gels. For FLight bioprinted constructs, however, collagen (mostly type II) was deposited in an aligned, columnar fashion, thus resembling articular cartilage deep-zone in its microarchitecture and composition. With 100% being the staining intensity of the human infant articular cartilage control, FLight samples reached ≈55%, ≈65%, and ≈85% of aggrecan, collagen II, and GAGs after 56 days of culture, respectively, while collagen I was found to be at lower concentration than the native tissue (≈50%) (Figure 3A-ii).

The amount of GAGs—one of the main articular cartilage components and a key player in tissue mechanics—and cell proliferation were assessed after 0, 28, and 56 days of culture (Figure 3B). Over these periods, no significant differences were observed in DNA when normalized to the construct weight between bulk or FLight. However, weight-normalized GAGs showed significant differences at 28 and 56 days, being ≈3 times higher for FLight than bulk hydrogels. When GAGs were normalized by DNA content, the ratio trended upward for both groups over time. The ratio increased more than 100-fold from day 0 to day 56 in FLight constructs, while a tenfold increase was observed in bulk constructs. In particular, considering that the GAGs/DNA ratio in the weight-bearing regions of human articular cartilage is ≈100 $\mu g\ \mu g^{-1}$,[52] the FLight-engineered cartilage essentially matched the native tissue after 56 days of culture ($\approx 102 \pm 1\ \mu g\ \mu g^{-1}$).

From an ECM composition standpoint, the histological analysis showed an excellent neocartilage formation for FLight constructs. However, it is known that the biomechanical properties of native articular cartilage are also closely coupled to the distinct zonal organization of the collagen fibers (Figure 1A). As mentioned above, from a first qualitative observation of SHG signals and collagen II immunostainings, it appears clear that a highly aligned (deep zone-like) collagen deposition took place in the anisotropic FLight hydrogels, as initially hypothesized. To corroborate these observations, polarized-light microscopy (PLM) on picrosirius red-stained slides was used to provide complementary information about the collagen fibers orientation, type and spatial distribution (**Figure 4**A). Bulk and FLight samples showed an increased picrosirius red staining intensity over culturing time, indicating a continuous neocartilage deposition by the embedded cells. Under PLM, birefringence gave information of collagen fiber thickness (red birefringence indicates

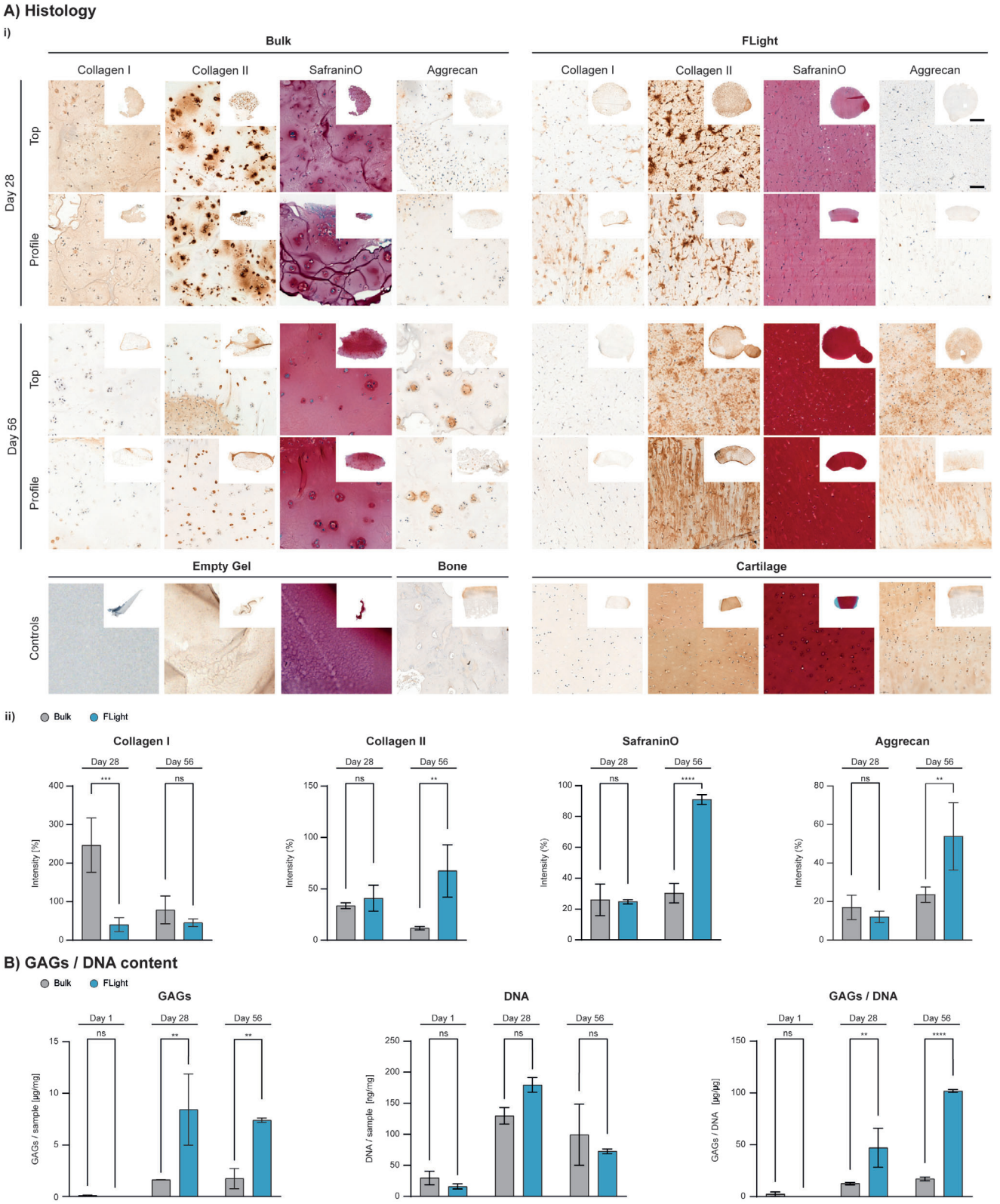

Figure 3. Characterization of neocartilage deposition. A-i) Histological and immunohistological staining of top and profile sections of FLight and bulk constructs over 28 and 56 days of culture for collagen I, collagen II, GAGs (SafraninO), and aggrecan. Controls of empty gels (without cells), bone (no aggrecan), and of human infant articular cartilage (bottom). Scale bar full sample: 1 mm. Scale bar close-up: 100 µm. ii) Comparison of staining intensities normalized to human infant articular cartilage (100%). B) Quantification of DNA and GAGs content in FLight and bulk samples after 1, 28, and 56 days of culture.

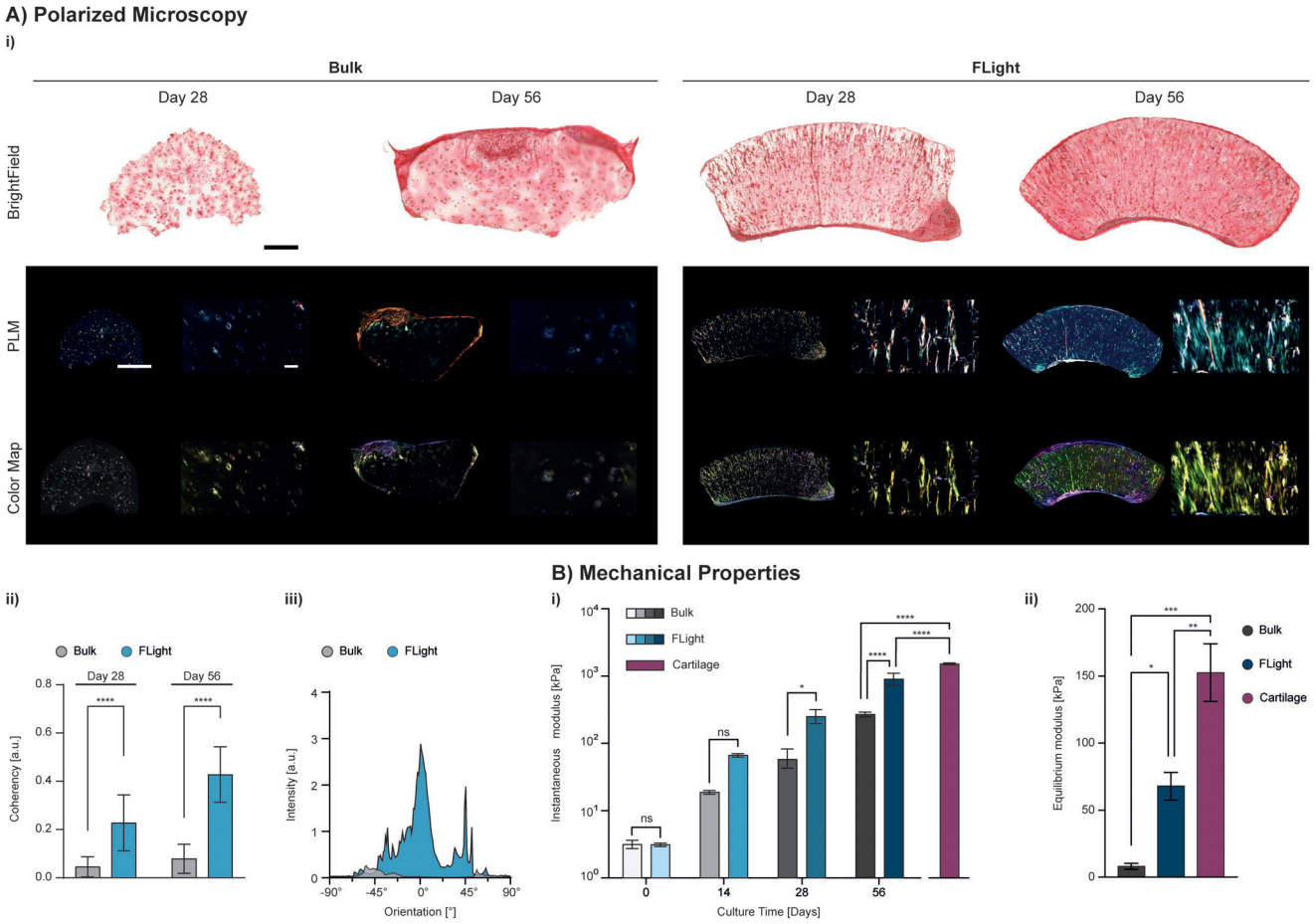

Figure 4. Evaluation of collagen fibrils alignment and mechanical properties characterization. A-i) Collagen staining by picrosirius red (Scale bar: 1 mm) allowed for the visualization of the spatial organization of the collagen network formed within the engineered constructs after 28 and 56 days in bulk and FLight conditions. The color map of the respective PLM images (mid row) obtained from the picrosirius red-stained slices is displayed in the bottom row showing clear collagen fibers and fibril alignment in the FLight condition (Scale bar: 1 mm, close ups: 50 µm). ii) Quantification of the collagen fibril coherency, with the value 1 indicating 100% alignment over the same angle/axis and 0 random distribution. iii) Fibrils' orientation displayed as distribution over angle (with 0° being perpendicular to construct top-bottom surfaces), showing strong directionality for the deposited collagen in FLight hydrogels and random orientation in the bulk gels. B-i) Mechanical properties of the engineered cartilage constructs assessed at different time points (0, 14, 28, and 56 days) by instantaneous compression modulus and ii) by equilibrium compression modulus after 56 days of culture.

thick fibers, mostly for collagen I, while green indicates thinner fibers/fibrils typical of collagen II).[53–55] In Flight gels PLM imaging showed the presence of sparse fibers (red-orange) after 28 days and a dense network of fibrils (green) after 56 days. Considering also the immunohistological finding reported in Figure 3, this compact network of aligned fibrils is mainly formed by collagen II.

On the other hand, PLM did not reveal a significant presence of collagen fibers/fibrils in the bulk gels. Only thick fibers surrounding the bulk gel were observed, probably deposited by cells growing on the surface of the construct. Moreover, while bulk samples did not show a distinct collagen orientation, a clear alignment was found in the anisotropic FLight constructs as particularly appreciable after the application of an orientation color map (Figure 4A-i). The color map was then used to quantify collagen fibril coherency and orientation (Figure 4A-ii), confirming a significant difference between the engineered constructs. FLight showed a significantly higher fibril coherency, with most fibrils aligned along the microfilament-microchannel axis (perpendicular to the hydrogel top and bottom surfaces).

Finally, matrix composition and architecture are key elements of articular cartilage that are also directly linked to the tissue's biomechanical properties. To determine how closely the engineered cartilage's mechanical properties approximated that of native cartilage, samples were tested under unconfined compression. As predicted by the cartilage-like ECM deposition found in histological staining, the instantaneous compressive modulus increased over the course of the culturing period (Figure 4B-i). Starting from relatively soft (≈5–7 kPa) gels at day 0, the instantaneous compression modulus eventually reached native cartilage-like values for FLight hydrogels (≈1 MPa) after 56 days. As far as we know, very few studies have achieved biomechanical properties rivaling native cartilage, and these often relied on high initial cell concentration or the presence of supporting structures.[56,57]

As expected from the less pronounced neocartilage deposition and absence of anisotropic ECM architecture, bulk gels reached

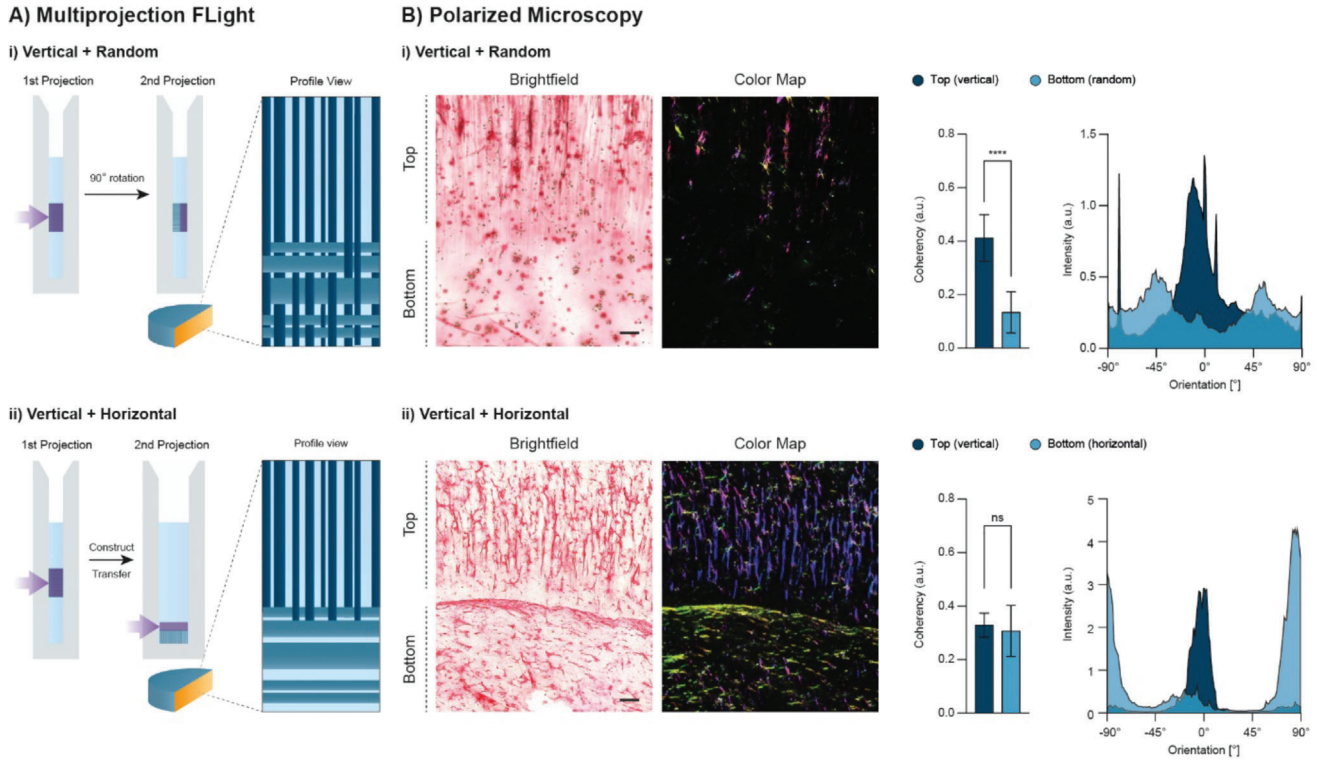

Figure 5. Evaluation of multiprojection FLight approach to direct collagen fibrils orientation in different directions. A) Schematic illustrating the procedures to obtain i) vertical+random and ii) vertical+horizontal bilayer constructs (see also Experimental Section). B) Collagen staining by pircrosirius red (left) and color map (right) of birefringence images taken by polarized microscopy Scale bars: 100 μm. On the right side quantification of the collagen fibrils coherency, with the value 1 indicating 100% alignment over the same angle/axis and 0 random distribution. Collagen fibrils orientation for the different zones in the two construct is also displayed as distribution over angle (0° being perpendicular to construct top-bottom surfaces and –90° and 90° being parallel to top-bottom surface).

a much lower stiffness value at day 56 (≈270 kPa). Notably, a similar stiffness was already achieved by the FLight hydrogels after only 28 days. In addition to the instantaneous modulus, we evaluated the equilibrium modulus. Interestingly, the equilibrium modulus of FLight samples was found to be half (≈75 kPa) of the cartilage control (≈150 kPa). This discrepancy is possibly related to an insufficient crosslinking of the collagen network. Studies have shown that the equilibrium modulus can be drastically increased through the addition of copper and/or lysl oxidase.[58,59]

In summary, these findings suggest that the anisotropic macroporous architecture granted by FLight biofabrication significantly improves articular cartilage tissue maturation remarkably approaching native composition, structure and biophysical properties. Importantly, although FLight showed overall promising results, it is important to note that this tissue engineering approach differs from native cartilage morphogenesis. In vivo articular cartilage formation arises from a complex sequence of intracellular and extracellular signals with spatiotemporal patterns that start from mesenchymal stem cells and lead to differentiated chondrocytes responsible for the ECM deposition.[60] The reorganization of chondrocytes in a columnar fashion in the deep zone then leads to the aligned collagen II deposition in forms of fibrils of tens to hundreds of nm in diameter. With our approach, embedded chondrocytes are facilitated in taking an aligned arrangement and depositing such fibrils in the aligned microchannels rather than randomly in the surrounding homogeneous matrix (bulk condition). However, as observed in Figure 4, this leads to an accumulation of thin collagen II fibrils mostly in the macroporous compartments which differs from the native pattern. Future research will need to unveil if this outcome is sufficient to match native cartilage performances in vivo or need further adjustments of printing technology, photoresin, cell choice, or culture conditions to even better resemble the native tissue.

2.3. Multiprojection FLight

The use of light projections ensures high printing flexibility as they guarantee spatiotemporal control over photocrosslinking and can be sent to the photoresin from different direction by simply using mirrors to deviate the light beam path. Therefore, we explored the possibility of using multiple consecutive projections using FLight mode to bioprint more structurally complex, multilayered hydrogels resembling the distinctive zones of articular cartilage. As proof-of-concept, multiprojection FLight (**Figure 5**A, see procedure details in Experimental Section) was used to generate bilayered hydrogels composed of a vertical zone (as seen in previous sections) and a second, random (Figure 5A-i, mesh of orthogonally oriented microchannels/microfilaments) or horizontal zone (Figure 5A-ii) mimicking middle and superficial zone,

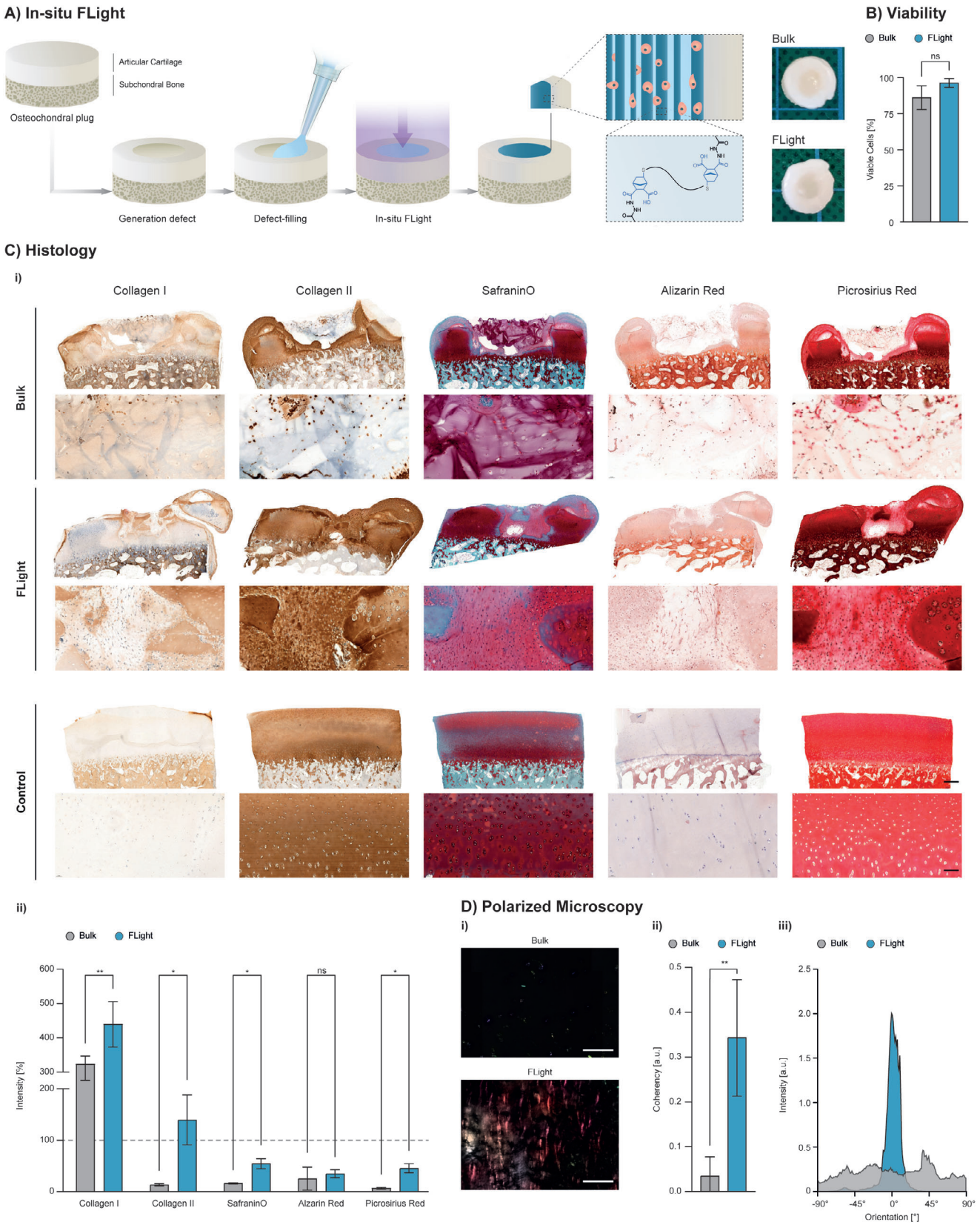

Figure 6. In situ FLight biofabrication of anisotropic hydrogels in cartilage defects. A) Illustration of cartilage defect preparation on osteochondral plugs, filled with hydrogel precursors and crosslinked with a top-down projection, obtaining in situ anisotropic articular cartilage. Corresponding images of the defects filled with gel and cultured over 56 days. B) Cell viability after 56 days of culture. C-i) Histological and immunohistological staining of profile

respectively. In the vertical+random condition, the constructs showed a clear distinction between the two zones in terms of collagen fibrils deposition after 56 days in culture, with vertically aligned fibrils on the vertical zone (top) and mainly pericellular deposition on the random zone (bottom) (picrosirius red staining, Figure 5B-i). Further analysis by polarized microscopy confirmed the significant differences between the two parts in terms of coherency and orientation. The multiprojection approach to obtain a vertical+horizontal bilayer construct showed instead a clear presence of highly coherent fibrils arranged vertically in the top layer (mimicking deep-zone) and horizontally in the bottom one (mimicking superficial zone) (Figure 5B-ii). These proof-of-concept results show another promising potential for FLight in cartilage tissue engineering and open to further research toward the generation even more complex multilayered systems and the implementation of automated, precise multiprojection systems to more closely resemble the native tissue in its structural complexity.

2.4. In Situ FLight

Finally, given these promising results, we explored in situ FLight as proof of principle for possible future clinical translation. As described above, FLight is a simple and extremely fast biofabrication technology based on light projection. In this first study, we adopted a cartilage-defect model based on bovine osteochondral plugs. The model consisted of a cartilage defect made with a 4 mm biopsy punch on the osteochondral plugs to mimic an articular cartilage lesion (**Figure 6**A). The optimized bioresin developed in this study (0.75% HA-NB/0.84% PEG2SH and 5 million cells mL^{-1} infant polydactyly chondrocytes) was then pipetted into the defect/damage site and FLight projection performed as previously described. Notably, as the photoresin acts as a liquid filler, in situ FLight can potentially be used to target any cartilage defect shape. The constructs (bulk and FLight) were maintained in culture for 56 days and then evaluated for their chondrogenesis. An optimal cell viability (>80%) was reported for both types of hydrogels after two months in culture (Figure 6B). Histological and immunohistological analysis confirmed the previous results, showing a significant difference between bulk and FLight (Figure 6C-i). A remarkable deposition of collagen II was reported for the in situ FLight samples, reaching the staining intensity found in human articular cartilage (100% value in the bar graph, Figure 6C-ii). On the other hand, as expected bulk hydrogel showed a mainly pericellular deposition of collagen I and II, and a lower (although not statistically significant) presence of GAGs. Interestingly, both bulk and FLight constructs showed a 3–4 times higher collagen I staining when compared to native tissue. This difference compared to the "hydrogel-only" study could be attributed to the use of the osteochondral plug set-up, as the presence of the bone cells underneath the printed constructs as well as damaged cartilage around them increases the biological complexity of the system (i.e., release of cytokines, growth factors) and could thus influence the chondrogenesis. However, there was no sign of tissue hypertrophy, as evidenced by the lack of mineralization shown in the alizarin red staining. Finally, PLM was exploited to assess the collagen orientation within the neocartilage, showing the presence of coherent and vertically aligned collagen fibers only for in situ FLight constructs (Figure 6D–i,ii,iii), mimicking the articular cartilage deep-zone. In conclusion, the macroporous architecture granted by FLight led to an anisotropic in situ maturation of articular cartilage with remarkable collagen II deposition, the main structural component of articular cartilage, at a level matching that found in native tissue.

3. Conclusion

We leveraged the unique capabilities of the novel FLight biofabrication technology and a high performance bioresin to generate articular cartilage constructs with composition, structure and mechanical properties similar to the native tissue. We foresee that these results will stimulate future work directed toward the possibility of fully reconstructing articular cartilage, featuring all different zones through applying projections in a multi-step procedure as preliminarily presented here, or by converging FLight with other bioprinting technologies. In addition, given the relatively simple set-up of FLight, this technology could be easily adopted by the tissue engineering community to explore further applications. Also, as previously demonstrated,[32,46] it is possible to tailor microfilament/channel size for a specific application by tuning optics (i.e., coherent length of the light beam) or material parameters (i.e., use of refractive index matching compounds such as iodixanol). The optical tuning of the photoresin refractive index can also be explored to reduce cell-induced scattering,[61,62] thus possibly increasing the initial cell concentration. Finally, we believe that the in situ FLight procedure could represent a valuable approach to repairing articular cartilage defects and damages. In particular, future studies will need to explore the possibility of using optical fibers for minimally invasive procedures. Among other things, strategies for overcoming the potential issue of the initial softness in load-bearing sites as well as the effect of the surrounding tissue on tissue maturation will need to be further investigated.

4. Experimental Section

All chemicals were purchased from Merck and cell culture reagents from Gibco unless indicated otherwise.

Synthesis of Hyaluronic Acid-Norbornene (HA-NB): Synthesis and characterization was performed as previously described by Rizzo et al.[44] 2.5 g (6.25 mmol, 1 eq.) of high molecular weight HA (1.5 MDa, HTL Biotechnology) was left to dissolve overnight, under stirring, in 1 L of 150 mM MES buffer pH 4.5. 5.45 g of adipic acid dihydrazide (ADH, 31.25 mmol, 5 eq.) was then added to the solution. Once completely dissolved, 300 mg of 1-Ethyl-3-(3-dimethylaminopropyl)carbodiimide (EDC, 1.56 mmol, 0.25 eq.) was solubilized in 2 mL of 150 mM MES buffer pH 4.5 and added dropwise to the reaction mixture. After 4 h the pH was found to be 4.72 and the

sections of bulk- and FLight-filled defects after 56 days of culture, and bovine osteochondral plug control for collagen I, collagen II, GAGs (SafraninO), calcification (alizarin red), and total collagens (picrosirius red). Scale bar full sample: 1 mm. Scale bar close-up: 100 µm. ii) Comparison of staining intensities normalized to human infant articular cartilage (100%). D-i) Color map of the respective PLM image obtained from the picrosirius red staining (Scale bar: 100 µm). ii) Coherency (with the value 1 indicating 100% alignment over the same angle/axis and 0 random distribution), and iii) orientation of collagen fibrils (with 0° being perpendicular to construct top-bottom surfaces).

reaction was quenched by addition of NaOH 1 M to reach pH 7. After the addition of 2 g of NaCl, the solution was dialyzed against mQ H2O for 5 days with frequent water changes and then freeze-dried. After lyophilization, 2.5 g of HA-ADH was left to dissolve overnight, under stirring, in 1 L of PBS pH 7.4. Then, 2 g of carbic anhydride (12.5 mmol, 2 eq.) was dissolved in 10 mL of DMF and added dropwise to the solution. The reaction was left to proceed for 8 h with pH adjustments every 30 min using NaOH 2 M to maintain pH 7.4. After addition of 2 g of NaCl the solution was dialyzed against mQ H2O for 3 days using a tangential flow filtration system (ÄKTA Flux, Cytiva) and then freeze-dried. HA-NB degree of substitution (DS) was found to be 18% with 1H-NMR (Bruker Ultrashield 400 MHz, 1024 scans) integrating for norbornene double bond peak (≈6.3 ppm). For NMR analysis, the high viscosity polymer was solubilized at 5 mg mL^{-1} in 1 mL of 2 mM NaCl D2O solution in the presence of a known amount of internal standard 3-(trimethylsilyl)-1-propanesulfonic acid (DSS). High ionic strength was found to be a powerful tool for improving the quality of the spectra. As reported by Ret et al., for long-chain, high viscosity polymers in particular, the control of their conformation in solution can determine better proton mobility.[63]

Cell Isolation and Expansion: Human infant chondrocytes were isolated as previously described[51] from the epiphyseal cartilage in joints removed during corrective surgery for polydactyly. A general consent or an informed consent was obtained from the legal guardians of polydactyly patients, and experiments were approved by the Ethical Committee of Canton Zürich (Kantonale Ethikkommission, Kanton Zürich, license PB_2017-00510). Isolated cells were plated at a concentration of 10 000 cells cm^{-2} and expanded in DMEM, 10% v/v FBS, 10 ng mL^{-1} FGF-2 and 10 µg mL^{-1} gentamicin until passage 3. At passage 3, cells were trypsinized, combined with DMEM, 10% v/v FBS, and 10 µg mL^{-1} gentamicin and collected by centrifugation (5 min, 400 rcf). Finally, the cell pellet was carefully mixed with the different hydrogel precursors at a concentration of 5 million cells mL^{-1}.

FLight Biofabrication: HA-NB was left to dissolve overnight under stirring in 150 mM NaCl 50 mM Tris buffer pH 7.4 at 1.2%. The polymer solution was then mixed with the addition of PEG2SH (5 kDa, JenKem Technology, 5% in 150 mM NaCl 50 mM Tris buffer pH 7.4) and LAP solution (2.5% in 150 mM NaCl, 50 mM Tris buffer, pH 7.4), to obtain the final HA-NB/PEG2SH (0.75% HA-NB, 0.84% PEG2SH, 0.05% LAP) photoresin formulation. The photoresin was then filter-sterilized (0.2 µm filter) and mixed with infant polydactyly chondrocytes (passage 3) to a final concentration of 5 million cells mL^{-1}. The resulting bioresin was pipetted (0.6 mL) into quartz cuvettes (2 mm depth, 1 cm wide, 3 cm height, CV10Q7FA, Thorlabs). FLight projections were executed in an open format volumetric printer (Readily3D) equipped with a collimated non-gaussian light beam from a Class IIIB laser (405 nm, 300 mW cm^{-2}) which was shaped into the desired projection cross-section using a digital micromirror device (DMD). The light path was customized with swappable mirrors enabling light projection from the side (standard mode) or top of the photoresin containing quartz cuvette. Projected images (10 × 4 mm discs) were designed in Adobe Illustrator 2022 and projected for 3.3 s. After printing, uncrosslinked resin was washed out using Tris buffer and samples were gently retrieved from the cuvettes using a spatula, then directly transferred to a 24-well plate with chondrogenic media (DMEM, 10 µg mL^{-1} gentamycin, 1% ITS+, 50 µg mL^{-1} L-ascorbate-2-phosphate, 40 µg mL^{-1} L-proline, and 10 ng mL^{-1} TGF-β3). The bulk samples, on the other hand, were casted in PDMS rings (4 mm diameter, 2 mm height) and crosslinked in a UV-box equipped with 405 nm LED strips (light intensity ≈6.8 mW cm^{-2}) for 30 s, thus matching FLight procedure light dose (≈208 mJ cm^{-2}). All samples were cultured in chondrogenic media in 24 well plates under gentle shaking with media change every 3 days.

Multiprojection FLight: Optimized bioresin (0.75% HA-NB / 0.84% PEG2SH / 0.05% LAP and 5 million cells mL^{-1} infant polydactyly chondrocytes) was prepared as previously described. For vertical-random bilayer (see Figure 5A-i), the photoresin was first crosslinked in a quartz cuvette (2 mm depth, 1 cm wide, 3 cm height, CV10Q7FA, Thorlabs) using a standard side projection (4 mm disc, 3.3 s). The cuvette was then rotated by 90° and a second side projection was directed toward approximately half of the printed construct (2 mm wide, 4 mm height projection for 3.3 s), thus forming a layer with a mesh of orthogonal microfilaments (random layer). For the vertical-horizontal printing (see Figure 5A-ii), after the first projection the construct was transferred to a second, larger cuvette (4 mm depth) and fresh bioresin was added on top. The second side projection (1 mm height rectangle, 3.3 s) was performed so to have a minimum overlap with the "vertical" construct and secure cohesion between the two layers.

In Situ FLight: Osteochondral grafts were obtained from a calf knee, and cartilage defects were made with a 4 mm biopsy punch. The optimized bioresin (0.75% HA-NB/0.84% PEG2SH/0.05% LAP and 5 million cells mL^{-1} infant polydactyly chondrocytes) was prepared as previously described and used to fill the cartilage defect. Using the customized printer a top-down projection was directed onto the osteochondral plug to crosslink the bioresin via FLight method. Bulk hydrogels were obtained via crosslinking in UV-box as previously described.

Microchannels/Microfilaments Infiltration Test and Characterization: Cell-free samples were fabricated as previously described using the bulk or FLight method. Samples were submerged in a solution of 1% FITC-Dextran (0.5 MDa) in PBS for 15 min prior to imaging on Leica TCS SP8 (Leica) confocal microscope. For FLight samples a *z*-stack of 100 µm (0.57 *z*-step) was taken to obtain a 3D reconstruction (Imaris) (Figure 1D-ii). Side and top sections were used to calculate the area distribution of channels and filaments using Fiji built-in functions and manually measure the size of the microfeatures, respectively.

Uniaxial Compression Tests: Uniaxial unconfined compression tests were performed on a TA.XTplus Texture Analyzer (Stable Micro Systems) equipped with a 500 g load cell. Samples were placed between the compression plates and pre-loaded (0.5 g at day 0, 2 g at day 14, 5 g at day 28, and 10 g at day 56) to ensure full contact with the plates. Samples were allowed to relax for 2 min and then compressed to 15% strain at 0.01 mm s^{-1}. Compressive modulus was calculated by linear fitting the stress-strain curve from 0.5% to 3% strain.

Instantaneous and equilibrium moduli were obtained from unconfined stress-relaxation compression tests. Samples were pre-loaded (0.05 N for empty gels and 0.25 N for day 56) to ensure full contact with the plates and then allowed to relax for 10 min. Afterward, 4 incremental intervals of 5% strain at a strain rate of 5% s^{-1} were applied. After the first and second interval, samples were held for 1800 s and after the third and fourth interval for 2700 s. Instantaneous modulus was calculated by fitting the loading curve between 15% and 20% strain and the equilibrium modulus calculated by linear fitting the stress–strain values at the end of each relaxation interval similar to those previously reported by Stok et al.[64]

Ellman's Test: HA-NB/PEG2SH photoresin was prepared as described above, casted into 4 mm-diameter PDMS molds and UV-crosslinked (405 nm, ≈208 mJ cm^{-2} light dose). The hydrogels were then submerged into a solution containing 100 µL of Ellman's reagent working solution (10 mM 5,5′-dithiobis-(2-nitrobenzoic acid) (DTNB) in 50 mM sodium acetate buffers mixt 2:7 with PBS pH 7.4 (Gibco). The solution absorbance was quantified at 412 nm. The amount of soluble PEG2SH present in the gel precursor solution was added to 100 µL of Ellman's working solution, as control, and the absorbance read at 412 nm. Then, the absorbance after photocrosslinking was divided by the initial total absorbance (normalized to 1) to know the percentage of free thiols after photocrosslinking (≈4%).

Swelling Ratio: HA-NB/PEG2SH photoresin was prepared as described above, casted into 4 mm-diameter PDMS molds, and UV-crosslinked (405 nm, ≈208 mJ cm^{-2} light dose). The hydrogels were then transferred to 1.5 mL Eppendorf tubes containing 1 mL PBS 1X. After 1 and 24 h, the supernatants were removed, and the samples weighted. The swelling ratio was determined as the ratio of hydrogel mass at 24 h divided by its initial mass at 1 h.

Live/Dead and Second Harmonic Generation (SHG) Imaging: Samples were biofabricated as previously described and incubated in FluoroBrite DMEM supplemented with 1:2000 CalceinAM (Invitrogen) and 1:500 Propidium Iodide (PI, Fluka) for 40 min. Imaging was then performed on a Leica SP8 microscope (Leica) equipped with a 25× objective. SHG imaging was collected at ≈450 nm with 900 nm two-photon excitation (Mai Tai laser, Spectra-Physics). Z-stacks were acquired from the sample surface at 2 µm steps and 100 µm into the sample. Gels were then cut with a

scalpel blade to image their profiles. The pictures reported in the work resulted from maximum intensity *z*-projection. Cell viability was assessed by counting viable (CalceinAM) and dead (PI) cells with the ImageJ Analyze particle function.

Gene Expression Analysis: Gene expression levels were assessed through real-time PCR (qPCR) analysis. Samples were first washed with Tris buffer and then snap-frozen in liquid N2. Frozen samples were mechanically disrupted with a pestle and then extraction of RNA was performed with NucleoZol (MachereyNagel) according to the manufacturer's instructions. Retrotranscription to cDNA was performed with GoScript Reverse Transcriptase (Promega) and cDNA was subsequently diluted 1:5 with RNAse-free water for qPCR analysis. The analyzed genes were Col2A1 (Fw: GGA ATT CGG TGT GGA CAT AGG, Rv: ACT TGG GTC CTT TGG GTT TG), Col1A1 (Fw: CAG CCG CTT CAC CTA CAG C, Rv: TTT TGTATT CAA TCA CTG TCT TGC C), Runx2 (Fw: CGC ATT TCA GGT GCT TCA GA, Rv: GCA TTC GTG GGT TGG AGA A), Sox9 (Fw: TCT GGA GAC TTC TGA ACG AGA GC, Rv: TGT AAT CCG GGT GGT CCT TC), ADAMTS5 (Fw: CGA TGG CAC TGA ATG TAG GC; Rv: CTC CGC ACT TGT CAT ACT GC), ACAN (Fw: GAA TGG GAA CCA GCC TAT ACC, Rv: TCT GTA CTT TCC TCT GTT GCTG), and normalized to GAPDH expression (Fw: AGT CAG CCG CAT CTT CTT TT, Rv: CCA ATA CGA CCA AAT CCG TTG). Quantitative real-time PCR (qPCR) was performed with GoTaq qPCR Master Mix (Promega) on a QuantStudio 3 device (Applied Biosystems).

Histology and Immunohistochemistry: Samples were washed in Tris buffer, fixed in 4% paraformaldehyde for 4 h and dehydrated in graded ethanol solutions. After fixation, bone-containing samples were decalcified in a weak acid solution (Evans and Krajian method) for three days with three changes per day and then dehydrated.[65] After dehydration, samples were paraffin-embedded and 5 µm sections (from top and profile) cut on a microtome. Before staining, samples were deparaffinized and rehydrated. Imaging was performed on an automated slide scanner (Panoramic 250, 3D Histech).

For Safranin O staining, samples were first stained in Weigert's Iron Hematoxylin solution for 5 min, followed by washing in deionized water and in 1% acid-alcohol for 2 s. Sections were washed again in deionized water, stained in 0.02% Fast Green solution for 1 min and rinsed with 1% acetic acid for 30 s. Finally, sections were stained in 1% Safranin O for 30 min, dehydrated with xylene and mounted.

For alizarin red, samples were stained with 2% alizarin red S in distilled water (pH adjusted to 4.1–4.3 with 10% ammonium hydroxide). Slides were then blotted, rinsed with 95% ethanol, dehydrated to xylene and mounted.

For picrosirius red staining, samples were first stained in Weigert's Iron Hematoxylin solution for 5 min, followed by washing in deionized water. Slides were then incubated for 1 h in 0.1% of Direct Red 80 in a saturated solution of picric acid. Finally, slides were washed in acidified water, dehydrated to xylene and mounted.

For immunohistochemistry (collagen I and collagen II stainings), antigen retrieval was performed with hyaluronidase (1200 U mL^{-1}) at 37 °C for 30 min. Sections were then blocked with 5% bovine serum albumin (BSA) in PBS for 1 h and then incubated overnight with the primary antibody, mouse anti collagen 1 (1:1000, Ab6308, abcam), mouse anti collagen 2 (1:20, Hybridoma Product II-II6B3, DSHB) or mouse anti aggrecan (1:100, 12/21/1-C-6 DSHB) in 1% BSA in PBS at 4 °C. Sections were then incubated with the secondary antibody, goat anti-rabbit IgG-HRP (1:1000, ab6789, abcam), in 1% BSA in PBS for 1 h and developed with the DAB substrate kit (ab64238, abcam) according to manufacturer's protocol for 5 min. Sections were stained with Weigert's iron hematoxylin (Thermo Fisher Scientific) for 3 min, destained in 1% acid-alcohol, blued in 0.1% Na2CO3, and finally dehydrated with xylene and mounted.

Slides were then imaged using 3DHistech slide scanner, while sections stained with picrosirius red were imaged using a Zeiss (AxioImager.Z2) polarized light microscopy. Analysis on the fiber orientation and coherency was carried out using the OrientationJ plugin in ImageJ software.[66]

Immunofluorescence: After 0, 7 or 14 days in culture the samples were washed 3× in PBS and fixed in 4% paraformaldehyde for 1 h at room temperature, followed by washing 3× in PBS. The samples were then permeabilized using a solution of 1% Triton-X100 in PBS for 10 min, followed by 1 h incubation with 1% BSA. Constructs were then incubated with primary antihuman Ki-67 antibody (350502, Biolegen), diluted 1:100 in PBS 1% BSA overnight. After washing 3× in PBS, the constructs were incubated with 1:100 fluorescent secondary antibody (goat antimouse Alexa488, Invitrogen), 1:1000 Hoechst 33342 (Invitrogen) and Phalloidin-TRITC (0.13 µg mL^{-1}, P1951, Sigma) in PBS with 1% BSA. Imaging was performed on a Leica SP8 confocal microscope (Leica) equipped with a 25× water immersion objective.

Sample Preparation for Biochemical Analysis: The scaffolds were washed with dH_2O, frozen at −80 °C and lyophilized overnight. Each sample was weighed before adding 500 µL of a 0.27 mg mL^{-1} solution of papain from Papaya Latex in a buffer containing 10 mM L-cysteine HCl, 100 mM sodium phosphate, and 10 mM EDTA in milliQ water, pH 6.3. The digestion was done at 60 °C overnight with shaking (1000 rpm).

DNA Quantification (Picogreen): The amount of DNA was quantified using a Quant-iT PicoGreen dsDNA assay kit (Invitrogen) per manufacturer's protocol. Briefly, the samples were pre-diluted 1:20 in TE buffer. 50 µL of this dilution was transferred into a 96-well plate and 50 µL of Picogreen solution was added. The fluorescence was measured with a micro-plate reader (excitation 480 nm, emission 520 nm). The DNA content was calculated as ng DNA per mg gel.

Glycosaminoglycans (GAGs) Quantification Assay: The GAGs amount was quantified using the Blyscan Glycosaminoglycan Assay on the digested samples. 50 µL of the samples were mixed with 0.5 mL of Blyscan dye reagent and incubated at room temperature for 30 min in a shaker. The samples were spun down at 12 000 rpm for 10 min. The supernatant was discarded, and 0.25 mL of dissociation reagent added. Finally, the samples were vortexed, centrifuged at 12 000 rpm for 5 min to remove the foam, and 100 µL were added to a 96-well plate. The absorbance was measured at 656 nm.

Osteochondral Explants: Osteochondral explants were harvested from bovine stifle joints of 3- to 5-month-old calves, obtained from a local abattoir (Angst AG, Zurich, CH). Osteochondral plugs were drilled, cleaned, and collected for culture.

Statistical Analyses: All statistical analyses were performed in GraphPad Prism version 9. A one-way ANOVA with Tukey's multi comparison test was used to analyze the data displayed in Figures 4B-ii, two-way ANOVA with multi comparisons for data displayed in Figures 2A-iii,B, 3A-ii,B, 4B-i, Figure S2 (Supporting Information), and unpaired *t*-test with Welch's correction was used to analyze the data displayed in Figures 1B-iii,D-iii, 5B, 6A–C-ii,D-ii, and Figure S1 (Supporting Information). A level of $p < 0.05$ was considered significant. Results were reported as mean ± standard deviation, the sample size for all experiments was $n = 3$.

Supporting Information

Supporting Information is available from the Wiley Online Library or from the author.

Acknowledgements

A.P.-J. and R.R. contributed equally to this work. M.Z.W. acknowledges Innosuisse funding application no. 55019.1 IP-ENG for their kind support. A.P. would like to thank the European Commission for providing financial support with the MSCA individual fellowship (Grant no: 885797). The authors acknowledge ETH ScopeM imaging facility for their assistance and Hao Liu and Dr. Parth Chansoria for their valuable inputs on FLight technology.

Conflict of Interest

The authors declare no conflict of interest.

Data Availability Statement

The data that support the findings of this study are openly available in ETH Repository at https://doi.org/10.3929/ethz-b-000610140, reference number 610140.

Keywords

alignment, bioprinting, cartilage, collagen, hyaluronic acid, light, photoclick

Received: October 3, 2023
Published online:

[1] J. Becerra, J. A. Andrades, E. Guerado, P. Zamora-Navas, J. M. López-Puertas, A. H. Reddi, *Tissue Eng., Part B* **2010**, *16*, 617.
[2] D. Correa, S. A. Lietman, *Semin. Cell Dev. Biol.* **2017**, *62*, 67.
[3] J. S. Temenoff, A. G. Mikos, *Biomaterials* **2000**, *21*, 431.
[4] B. Balakrishnan, R. Banerjee, *Chem. Rev.* **2011**, *111*, 4453.
[5] J. Yang, Y. S. Zhang, K. Yue, A. Khademhosseini, *Acta Biomater.* **2017**, *57*, 1.
[6] C. Chung, J. A. Burdick, *Adv. Drug Delivery Rev.* **2008**, *60*, 243.
[7] J. Antons, M. G. M. Marascio, J. Nohava, R. Martin, L. A. Applegate, P. E. Bourban, D. P. Pioletti, *J. Mater. Sci.: Mater. Med.* **2018**, *29*, 57.
[8] A. R. Poole, T. Kojima, T. Yasuda, F. Mwale, M. Kobayashi, S. Laverty, *Clin. Orthop. Relat. Res.* **2001**, *391*, 391.
[9] C. A. Baumann, B. B. Hinckel, C. C. Bozynski, J. Farr, In *Joint Preservation of the Knee: A Clinical Casebook* (Eds.: A. B. Yanke, B. J Cole), Springer Nature, Switzerland **2019**, pp. 3–24.
[10] A. M. Seitz, D. Warnecke, L. Dürselen, In *Human Orthopaedic Biomechanics* (Eds.: B. Innocenti, F. Galbusera), Academic Press, Switzerland **2022**, pp. 151–176.
[11] N. Broguiere, E. Cavalli, G. M. Salzmann, L. A. Applegate, M. Zenobi-Wong, *ACS Biomater. Sci. Eng.* **2016**, *2*, 2176.
[12] P. Fisch, N. Broguiere, S. Finkielsztein, T. Linder, M. Zenobi-Wong, *Adv. Funct. Mater.* **2021**, *31*, 2008261.
[13] K. Flégeau, A. Puiggali-Jou, M. Zenobi-Wong, *Biofabrication* **2022**, *14*, 034105.
[14] A. Puiggalí-Jou, M. Asadikorayem, K. Maniura-Weber, M. Zenobi-Wong, *Acta Biomater.* **2023**, *166*, 69.
[15] J. A. M. Steele, A. C. Moore, J.-P. St-Pierre, S. D. Mccullen, A. J. Gormley, C. C. Horgan, C. R. M. Black, C. Meinert, T. Klein, S. Saifzadeh, R. Steck, J. Ren, M. A. Woodruff, M. M. Stevens, *Biomaterials* **2022**, *286*, 121548.
[16] J. M. Coburn, M. Gibson, S. Monagle, Z. Patterson, J. H. Elisseeff, *Proc. Natl. Acad. Sci. U. S. A.* **2012**, *109*, 10012.
[17] S. D. Mccullen, H. Autefage, A. Callanan, E. Gentleman, M. M. Stevens, *Tissue Eng., Part A* **2012**, *18*, 2073.
[18] X. Barceló, K. F. Eichholz, I. F. Gonçalves, O. Garcia, D. J. Kelly, *Acta Biomater.* **2023**, *158*, 216.
[19] A. Bhattacharjee, D. S. Katti, *ACS Biomater. Sci. Eng.* **2019**, *5*, 114.
[20] Y. Zhang, F. Yang, K. Liu, H. Shen, Y. Zhu, W. Zhang, W. Liu, S. Wang, Y. Cao, G. Zhou, *Biomaterials* **2012**, *33*, 2926.
[21] Y. Shen, Y. Xu, B. Yi, X. Wang, H. Tang, C. Chen, Y. Zhang, *Biomacromolecules* **2021**, *22*, 2284.
[22] T. J. Levingstone, A. Matsiko, G. R. Dickson, F. J. O'brien, J. P. Gleeson, *Acta Biomater.* **2014**, *10*, 1996.
[23] B. Wang, F. Chariyev-Prinz, R. Burdis, K. Eichholz, D. J. Kelly, *Biofabrication* **2022**, *14*, 024101.
[24] R. Burdis, F. Chariyev-Prinz, D. C. Browe, F. E. Freeman, J. Nulty, E. E. Mcdonnell, K. F. Eichholz, B. Wang, P. Brama, D. J. Kelly, *Biomaterials* **2022**, *289*, 121750.
[25] D. C. Browe, P. J. Díaz-Payno, F. E. Freeman, R. Schipani, R. Burdis, D. P. Ahern, J. M. Nulty, S. Guler, L. D. Randall, C. T. Buckley, P. A. J. Brama, D. J. Kelly, *Acta Biomater.* **2022**, *143*, 266.
[26] M. E. Prendergast, M. D. Davidson, J. A. Burdick, *Biofabrication* **2021**, *13*, 044108.
[27] M. E. Prendergast, S.-J. Heo, R. L. Mauck, J. A. Burdick, *Biofabrication* **2023**, *15*, 035003.
[28] R. Rizzo, A. Bonato, P. Chansoria, M. Zenobi-Wong, *ACS Biomater. Sci. Eng.* **2022**, *8*, 3871.
[29] J. P. K. Armstrong, E. Pchelintseva, S. Treumuth, C. Campanella, C. Meinert, T. J. Klein, D. W. Hutmacher, B. W. Drinkwater, M. M. Stevens, *Adv. Healthcare Mater.* **2022**, *11*, 2200481.
[30] C. Gegg, F. Yang, *Acta Biomater.* **2020**, *101*, 196.
[31] A. Arora, A. Kothari, D. S. Katti, *J. Mech. Behav. Biomed. Mater.* **2015**, *51*, 169.
[32] H. Liu, P. Chansoria, P. Delrot, E. Angelidakis, R. Rizzo, D. Rütsche, L. A. Applegate, D. Loterie, M. Zenobi-Wong, *Adv. Mater.* **2022**, *34*, 2204301.
[33] M. Lee, R. Rizzo, F. Surman, M. Zenobi-Wong, *Chem. Rev.* **2020**, *120*, 10950.
[34] E. Öztürk, Ø. Arlov, S. Aksel, L. Li, D. M. Ornitz, G. Skjåk-Bræk, M. Zenobi-Wong, *Adv. Funct. Mater.* **2016**, *26*, 3649.
[35] J. H. Galarraga, R. C. Locke, C. E. Witherel, B. D. Stoeckl, M. Castilho, R. L. Mauck, J. Malda, R. Levato, J. A. Burdick, *Biofabrication* **2022**, *14*, 014106.
[36] L. Bian, C. Hou, E. Tous, R. Rai, R. L. Mauck, J. A. Burdick, *Biomaterials* **2013**, *34*, 413.
[37] M. Müller, E. Öztürk, Ø. Arlov, P. Gatenholm, M. Zenobi-Wong, *Ann. Biomed. Eng.* **2017**, *45*, 210.
[38] E. Öztürk, T. Stauber, C. Levinson, E. Cavalli, Ø. Arlov, M. Zenobi-Wong, *Biomed. Mater.* **2020**, *15*, 045019.
[39] M. Y. Kwon, C. Wang, J. H. Galarraga, E. Puré, L. Han, J. A. Burdick, *Biomaterials* **2019**, *222*, 119451.
[40] F. Boschetti, G. Pennati, F. Gervaso, G. M. Peretti, G. Dubini, *Biorheology* **2004**, *41*, 159.
[41] J. M. Patel, B. C. Wise, E. D. Bonnevie, R. L. Mauck, *Tissue Eng., Part C* **2019**, *25*, 593.
[42] D. L. Robinson, M. E. Kersh, N. C. Walsh, D. C. Ackland, R. N. De Steiger, M. G. Pandy, *J. Mech. Behav. Biomed. Mater.* **2016**, *61*, 96.
[43] C. F. Guimarães, L. Gasperini, A. P. Marques, R. L. Reis, *Nat. Rev. Mater.* **2020**, *5*, 351.
[44] R. Rizzo, N. Petelinsek, A. Bonato, M. Zenobi-Wong, *Adv. Sci.* **2023**, *10*, 2205302
[45] R. Rizzo, D. Ruetsche, H. Liu, M. Zenobi-Wong, *Adv. Mater.* **2021**, *33*, 2102900.
[46] R. Rizzo, D. Rütsche, H. Liu, P. Chansoria, A. Wang, A. Hasenauer, M. Zenobi-Wong, *Adv. Mater. Technol.* **2023**, *8*, 2201871.
[47] J. Farr, J. Q. Yao, *Cartilage* **2011**, *2*, 346.
[48] F. L. Acosta, L. Metz, H. D. Adkisson, J. Liu, E. Carruthers-Liebenberg, C. Milliman, M. Maloney, J. C. Lotz, *Tissue Eng., Part A* **2011**, *17*, 3045.
[49] H. D. Adkisson, J. A. Martin, R. L. Amendola, C. Milliman, K. A. Mauch, A. B. Katwal, M. Seyedin, A. Amendola, P. R. Streeter, J. A. Buckwalter, *Am. J. Sports Med.* **2010**, *38*, 1324.
[50] H. D. Adkisson, C. Milliman, X. Zhang, K. Mauch, R. T. Maziarz, P. R. Streeter, *Stem Cell Res.* **2010**, *4*, 57.
[51] E. Cavalli, C. Levinson, M. Hertl, N. Broguiere, O. Brück, S. Mustjoki, A. Gerstenberg, D. Weber, G. Salzmann, M. Steinwachs, G. Barreto, M. Zenobi-Wong, *Sci. Rep.* **2019**, *9*, 4275.
[52] B. A. Rogers, C. L. Murphy, S. R. Cannon, T. W. R. Briggs, *J. Bone Jt. Surg., Br. Vol.* **2006**, *88-B*, 1670.
[53] H. K. Gahunia, K. P. H. Pritzker, In *Articular Cartilage of the Knee: Health, Disease and Therapy* (Eds.: H. K. Gahunia, A. E. Gross, K. P. H. Pritzker, P. S. Babyn, L. Murnaghan), Springer, New York **2020**, pp. 3–70.

[54] R. Lattouf, R. Younes, D. Lutomski, N. Naaman, G. Godeau, K. Senni, S. Changotade, *J. Histochem. Cytochem.* **2014**, *62*, 751.
[55] L. C. U. Junqueira, G. Bignolas, R. R. Brentani, *Histochem. J.* **1979**, *11*, 447.
[56] B. J. Bielajew, R. P. Donahue, E. K. Lamkin, J. C. Hu, V. C. Hascall, K. A. Athanasiou, *Biomater. Res.* **2022**, *26*, 34.
[57] A. D. Cigan, B. L. Roach, R. J. Nims, A. R. Tan, M. B. Albro, A. M. Stoker, J. L. Cook, G. Vunjak-Novakovic, C. T. Hung, G. A. Ateshian, *J. Biomech.* **2016**, *49*, 1909.
[58] E. A. Makris, R. F. Macbarb, D. J. Responte, J. C. Hu, K. A. Athanasiou, *FASEB J.* **2013**, *27*, 2421.
[59] E. A. Makris, D. J. Responte, N. K. Paschos, J. C. Hu, K. A. Athanasiou, *Proc. Natl. Acad. Sci. U. S. A.* **2014**, *111*, E4832.
[60] Z. Wu, S. H. Korntner, A. M. Mullen, D. I. Zeugolis, *Biomater. Biosyst.* **2021**, *4*, 100030.
[61] P. N. Bernal, M. Bouwmeester, J. Madrid-Wolff, M. Falandt, S. Florczak, N. G. Rodriguez, Y. Li, G. Größbacher, R.-A. Samsom, M. van Wolferen, L. J. W. van der Laan, P. Delrot, D. Loterie, J. Malda, C. Moser, B. Spee, R. Levato, *Adv. Mater.* **2022**, *34*, 2110054.
[62] S. You, Y. Xiang, H. H. Hwang, D. B. Berry, W. Kiratitanaporn, J. Guan, E. Yao, M. Tang, Z. Zhong, X. Ma, D. Wangpraseurt, Y. Sun, T.-Y. Lu, S. Chen, *Science Advances* **2023**, *9*, eade7923.
[63] D. Ret, G. Steiner, S. Gentilini, S. Knaus, *Carbohydr. Polym.* **2019**, *204*, 124.
[64] K. S. Stok, G. Lisignoli, S. Cristino, A. Facchini, R. Müller, *J. Biomed. Mater. Res., Part A* **2010**, *93A*, 37.
[65] E. A. Wallington, *Histological Methods for Bone*, Butterworths, London **1972**.
[66] R. Rezakhaniha, A. Agianniotis, J. T. C. Schrauwen, A. Griffa, D. Sage, C. V. C. Bouten, F. N. Van De Vosse, M. Unser, N. Stergiopulos, *Biomech. Model. Mechanobiol.* **2012**, *11*, 461.